DESDE 2013
https://repository.uaeh.edu.mx/revistas/index.php/icbi/issue/archive
Pädi Boletín Científico de Ciencias Básicas e Ingenierías del ICBI
ISSN: 2007-6363

Publicación Semestral Pädi Vol. 13 No. Especial 4 (2025) 201-206

Vanadium oxide (V_xO_y) thin films obtained by pulsed laser deposition
Películas delgadas de óxidos de vanadio (V_xO_y) obtenidas por depósito por láser pulsado

L. Escobar-Alarcón[a,*], D. Fuentes-Molina[b], L.A. Martínez-Chávez[b], K. Esquivel[b], D.A. Solis-Casados[c]

[a] *Departamento de Física, Instituto Nacional de Investigaciones Nucleares, Carretera México-Toluca S/N, la Marquesa, Ocoyoacac, Estado de México. C.P.52750 México.*
[b] *División de Investigación y Posgrado, Facultad de Ingeniería, Universidad Autónoma de Querétaro, Cerro de las Campanas, Santiago de Querétaro, Querétaro 76010, México.*
[c] *Universidad Autónoma del Estado de México, Facultad de Química, Centro Conjunto de Investigación en Química Sustentable UAEM-UNAM, México.*

Abstract
Vanadium oxide thin films were successfully deposited onto glass substrates using the pulsed laser deposition (PLD) technique from a high-purity vanadium target. Structural and physicochemical characterizations by Raman and X-ray photoelectron spectroscopy (XPS) confirmed the coexistence of vanadium pentoxide (V_2O_5), vanadium dioxide (VO_2), possibly vanadium oxide nanotubes, and sodium vanadate ($NaVO_3$). Scanning electron microscopy revealed microneedles, microbars, and nanotube-like morphologies, while UV-Vis diffuse reflectance spectroscopy indicated both direct and indirect optical transitions, with band gap values influenced by the coexistence of mixed phases. Photoluminescence spectra displayed emission lines attributable to V_2O_5. These results highlight the versatility of PLD for producing multifunctional vanadium oxide films with mixed oxidation states and controlled morphology, avoiding chemical precursors and providing a sustainable route toward applications in photocatalysis, smart windows, solar cells, and optoelectronic devices.

Keywords Vanadium Oxides, Pulsed Laser Deposition, Thin Films.

Resumen
Se depositaron con éxito películas delgadas de óxido de vanadio sobre sustratos de vidrio mediante la técnica de depósito por láser pulsado (PLD) a partir de un blanco de vanadio de alta pureza. Las caracterizaciones estructurales y fisicoquímicas mediante espectroscopía fotoelectrónica de rayos X (XPS) y Raman confirmaron la coexistencia de pentóxido de vanadio (V_2O_5), dióxido de vanadio (VO_2), posiblemente nanotubos de óxido de vanadio y vanadato de sodio ($NaVO_3$). La microscopía electrónica de barrido reveló microagujas, microbarras y morfologías similares a nanotubos, mientras que la espectroscopía de reflectancia difusa UV-Vis indicó transiciones ópticas tanto directas como indirectas, con valores de banda prohibida influenciados por la coexistencia de mezclas de fases. Los espectros de fotoluminiscencia mostraron líneas de emisión atribuibles al V_2O_5. Estos resultados resaltan la versatilidad de PLD para producir películas multifuncionales de óxido de vanadio con estados de oxidación mezclados y morfología controlada, evitando precursores químicos y proporcionando una ruta sostenible hacia aplicaciones en fotocatálisis, ventanas inteligentes, celdas solares y dispositivos optoelectrónicos.

Palabras Clave: Óxidos de Vanadio, Depósito por Láser Pulsado, Películas Delgadas.

1. Introduction

Vanadium is a transition metal, discovered by a Spanish-Mexican scientist in Zimapán, Hidalgo, Mexico in 1801. This metal with multiple oxidation states, forms a wide variety of vanadium oxides such as V_2O_5, VO_2, V_2O_3, and VO corresponding to the +5, +4, +3 and +2 oxidation states respectively. It can also form oxides that combine oxidation states, e.g. V_6O_{13} (V^{5+}/V^{4+}), V_8O_{15}, V_7O_{13}, V_6O_{11} (V^{4+}/V^{3+}) (Barceloux and Barceloux, 1999). Thus, vanadium oxides constitute an important family of materials with diverse crystal structures and physicochemical properties (Liu et al., 2007). These materials exhibit metallic, semiconducting, and insulating behavior, enabling applications in a variety of technological areas (Hu et al., 2023), such as photocatalysis (Pooseekheaw et al., 2022), water treatment (Gonzalez-Zavala *et al.*, 2016), Li-ion batteries (Mai *et al.*, 2011 Julien et al 2001), and solar cells (Chen *et al.*, 2019).

*Autor para la correspondencia: luis.escobar@inin.gob.mx
Correo electrónico: dfuentes12@alumnos.uaq.mx (David Fuentes Molina), luis.alejandro.martinez@uaq.edu.mx (Luis Alejandro Martínez Chávez), karen.esquivel@uaq.mx (Karen Esquivel Escalante), solis_casados@yahoo.com.mx (Dora Alicia Solis Casados), luis.escobar@inin.gob.mx (Luis Escobar Alarcón)

Historial del manuscrito: recibido el 05/09/2025, última versión-revisada recibida el 31/10/2025, aceptado el 05/11/2025, publicado el 12/12/2025. **DOI:** https://doi.org/10.29057/icbi.v13iEspecial4.12548

Vanadium dioxide (VO_2) and vanadium pentoxide (V_2O_5), two thermodynamically stable phases, with band gaps of ~0.6 and ~2.3 eV, respectively, have been widely studied as chromogenic materials because their optical properties respond to external stimuli such as electromagnetic radiation, electric charge, or heat, which makes them suitable for optoelectronics and solar cells for energy saving windows applications (Bahlawane and Lenoble, 2014). Among chromogenic materials, thermochromic materials constitute a subcategory that changes their properties in response to temperature variations. This response is passive, as it is driven by ambient temperature rather than user intervention (Aburas *et al.*, 2019).

VO_2 has been proposed as a thermochromic material owing to its relatively very low transition temperature (T_c) of 68°C, from semiconductor to metal behavior, which enables modulation of incident light and reduces infrared transmittance (Wang *et al*., 2016). Numerous studies have lowered the T_c by doping VO_2 with elements such as molybdenum (Zhang *et al*., 2012), tungsten (Salamati *et al.*, 2019), and boron (Zhou *et al*., 2020), achieving a minimum T_c of 28.1°C. In contrast, V_2O_5 exhibits highly anisotropic electrical and optical properties. The T_c of crystalline V_2O_5 thin films occurs at approximately 257°C (Aita *et al*., 1986). The monocrystalline V_2O_5 (001) surface in thin film form can undergo a reversible transition between 77-127 °C that is confined to the surface layer; bulk V_2O_5 does not show this behavior (Blum *et al*., 2007). Consequently, V_2O_5 thin films are promising for various applications, including optical and electrical switching, thermochromic devices, and thermal sensors (Bannuru *et al*., 2008).

Among thin film formation methods, pulsed laser deposition (PLD) is a powerful and versatile technique for preparing thin films with tailored properties which can have a wide range of potential applications. In this line, our group has been working in the implementation of several experimental configurations to develop thin films for photocatalysis under simulated solar irradiation (Gonzalez-Zavala, *et al.*, 2016; Escobar-Alarcón *et al.*, 2024), Li-ion micro-batteries (Julien *et al*., 1999), high-hardness coatings (Escobar-Alarcón *et al*., 2005), and surface enhanced Raman spectroscopy (Morales Méndez *et al*., 2023), among others. In this work, we present results on the deposition and characterization of vanadium oxide thin films prepared by PLD. Thin films were characterized by several techniques to know their physical and chemical properties. X-ray photoelectron spectroscopy (XPS) was used to determine the elemental chemical composition and the oxidation state of the elements present; UV-Vis spectroscopy was used to determine the band gap energy, the microstructure was characterized by micro-Raman spectroscopy, the surface morphology was examined by scanning electron microscopy (SEM) and Photoluminescence was employed to determine the defects present in the material.

2. Experimental

2.1. Thin film deposition

Vanadium oxide thin films were deposited by PLD on glass substrates (2.5 x 2.5 cm). The target was a high-purity vanadium disk (99.99%) with a diameter of 2.54 cm and a thickness of 0.63 cm. It was ablated with a Nd: YAG laser (1064 nm, 5 ns pulse duration) operating at 10 Hz. Depositions were carried out at 3×10^{-4} Torr, with a target-substrate distance of 5 cm. The deposition time was 60 min for all samples. Films were prepared at three laser fluences: 7.3, 13.3 and 30.6 J/cm^2. After deposition, the films were subjected to a thermal treatment at 450°C for 3 hours in an open-atmosphere furnace to completely oxidize any remaining metallic vanadium and to improve crystallinity. The samples exhibited yellowish to reddish-brown colors, consistent with vanadium oxides.

2.2. Physicochemical characterization

Raman spectra were acquired with a micro-Raman system equipped with an Olympus BX40 confocal microscope. The 532 nm line of a Nd:YAG laser was used, and two positions were measured on each film. Surface morphology was examined with a JEOL JSM 6510LV scanning electron microscope (SEM). X-ray photoelectron spectroscopy (XPS) was performed with a Thermo Scientific K-alpha XPS spectrometer, to determine surface composition and oxidation states. Photoluminescence (PL) spectra were collected on a Horiba Jobin Yvon FluoroMax-4 spectrofluorometer using a 500 nm excitation. Diffuse reflectance UV-Vis spectra were obtained with a Varian Cary 100 Conc spectrophotometer to estimate optical properties.

3. Results and discussion

3.1. SEM characterization

SEM images (Figure 1) show that the film deposited at the lowest fluence (7.3 J/cm^2) presents agglomerated needle-shaped micrometer-scale structures (Figure 1a). A closer view reveals two-dimensional arrangements formed by ordered agglomeration of needles which are aligned, by group, in the same direction (Figure 1b). The sample deposited at 13.3 J/cm^2 shows individual needles dispersed on the surface with little agglomeration (Figure 1c); higher magnification reveals microbars approximately 20 μm in length (Figure 1d). For the sample prepared at 30.6 J/cm^2, in addition to microscale droplets, some needles are observed (Figure 1e), and at a higher magnification nanoribbons or nanotubes are evident (Figure 1f). All three films display needle-like morphologies, suggesting a common vanadium oxide phase, and the possible formation of vanadium oxide nanotubes, consistent with reported elongated, needle-like nanotube morphologies characteristic of vanadium oxide with outer diameters of 15-100 nm (Muhr *et al*., 2000).

3.2. Microstructural characterization

Raman spectra corresponding to the sample prepared at 7.3 J/cm^2 are very similar in the two different points measured (Figure 2a). Features at 87, 112, 136, 196, 288, 320, 476, and

992 cm^{-1} are assigned to the vibrational modes of vanadium pentoxide (V_2O_5) (Liu *et al*., 2006; Ureña-Begara *et al.*, 2017). Signals at 223, 254, and 430 cm^{-1} correspond to vanadium dioxide (VO_2) (Schilbe, 2002; Pan *et al*., 2004; Théry *et al*., 2016). Bands at 170, 805, 885, and 912 cm^{-1} are consistent with V_7O_{16} nanotubes (Julien, *et al*., 1997; Ureña-Begara, *et al.*, 2017). Peaks at 429, 556, 731, 886, 909, and 943 cm^{-1} indicate $NaVO_3$ (Utegulov *et al*., 2003; Neuville, 2006).

Raman spectra of the 13.3 J/cm² sample are also similar at both measurement positions (Figure 2b). V_2O_5 bands appear at 84, 110, 136, 192, 277, 304, and 480 cm^{-1} (Liu *et al*., 2006; Ureña-Begara *et al*., 2017). Signals at 220, 255, 503, 594 and 672 cm^{-1} are assigned to VO_2 (Schilbe, 2002; Pan *et al*., 2004; Théry *et al*., 2016); while features at 160, 255, and 809 cm^{-1} are consistent with V_7O_{16} nanotubes (Julien, *et al*., 1997; Ureña-Begara, *et al*., 2017). Low intensity peaks at 429 and 731 cm^{-1} can be attributed to $NaVO_3$ (Utegulov *et al*., 2003; Neuville, 2006). Different Raman spectra were obtained for the film prepared at 30.6 J/cm², indicating a non-uniform phase distribution (Figure 2c). V_2O_5 signals are located at 107, 137, 198, 282, 510, and 992 cm^{-1} (Liu *et al*., 2006; Ureña-Begara, *et al*, 2017). VO_2 bands occur at 262, 344, 430, 603, and 668 cm^{-1} (Schilbe, 2002; Pan *et al*., 2004; Théry *et al*., 2016). Vibrational modes at 170, 885, 916, and 940 cm^{-1} may arise from V_7O_{16} nanotubes (Julien *et al*., 1997; Ureña-Begara *et al*., 2017). Low intensity peaks at 430, 635, 886, 916, and 954 cm^{-1} are attributed to $NaVO_3$ (Utegulov *et al*., 2003; Neuville, 2006). Overall, Raman results indicate that the films consist of mixtures of different vanadium-oxide phases.

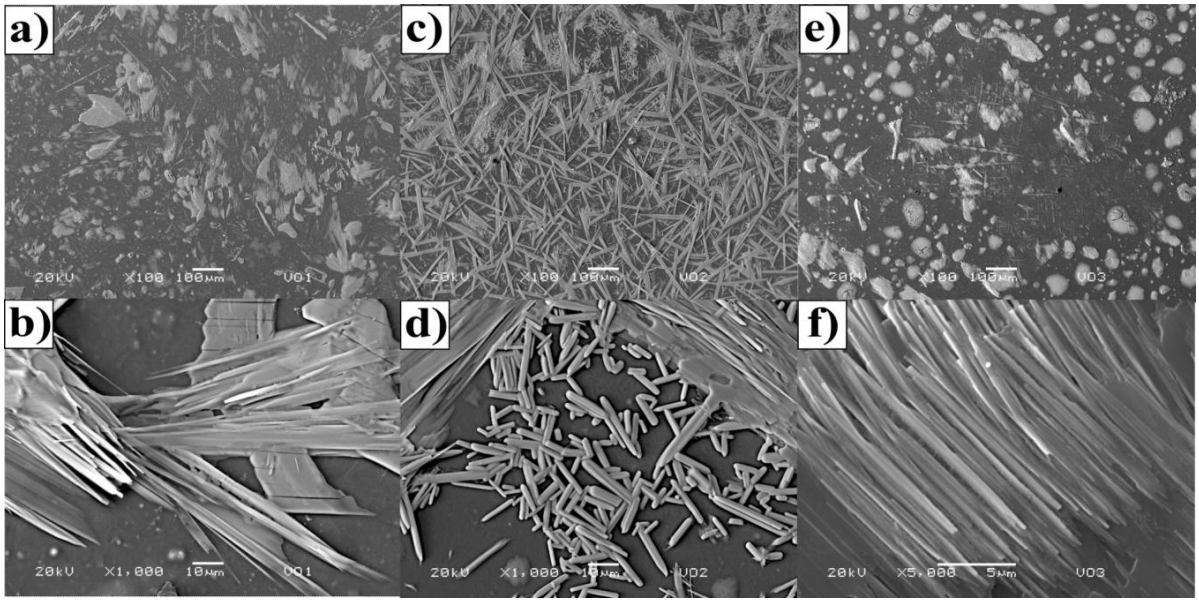

Figure 1. SEM images at 100× and 1000× of films deposited at laser fluences of 7.3 J/cm² (a,b), 13.3 J/cm² (c,d), and 30.6 J/cm² (e,f).

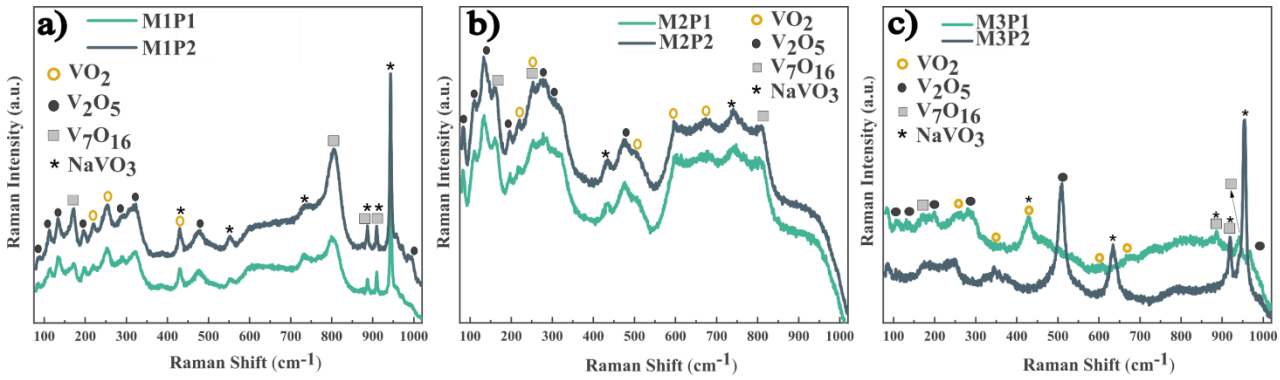

Figure 2. Raman spectra for films deposited at 7.3 J/cm² (a), 13.3 J/cm² (b) and 30.6 J/cm² (c). P1 and P2 refer to the different points in which Raman measurements were performed.

3.3. XPS Characterization

Figure 3a shows the high-resolution XPS spectra for the sample deposited at 7.3 J/cm² in the region from 540 to 510 eV, which includes the O1s and the V2p orbitals. Four peaks are observed close to 533, 530, 524, and 517 eV. The first two correspond to the O1s, while the last two correspond to the $V2p_{1/2}$ and $V2p_{3/2}$ doublet. For a detailed analysis the peaks were fitted using Voigt profile line shapes. In the O1s region, components at 533.4 and 531.1 eV are assigned to Si–O (SiO_2) and O–V bonds, respectively. In the V2p region, two doublets are present: 524.8 and 517.9, and 523.4 and 516.0 eV, corresponding to V^{5+} and V^{4+} oxidation states respectively (Moulder *et al*., 1992; Ureña-Begara *et al*., 2017).

These results suggest a mixture of V^{4+} and V^{5+} composing the film. Additionally, it is observed that the signal corresponding to the V^{5+} state (V_2O_5) is of higher intensity than the V^{4+} (VO_2), indicating a higher amount of V_2O_5 on the surface of this sample. The shape of the $V2p_{1/2}$ and $V2p_{3/2}$ signals is bell-shaped with a broad base. It has been reported that the presence of V^{4+} decreases the slope of the signals corresponding to V_2O_5 (Mendialdua *et al.*, 1995).

In Figure 3b, the XPS high-resolution spectrum of the film prepared at 13.3 J/cm^2 is presented. The same features are observed with intensity changes: the Si–O component is weaker relative to O–V, and the V^{5+} signal increases relative to V^{4+}, indicating a higher V_2O_5 fraction. Notably, vanadium-oxide nanotubes typically contain V^{4+} and V^{5+} oxidation states mixed (Souza Filho *et al.*, 2004).

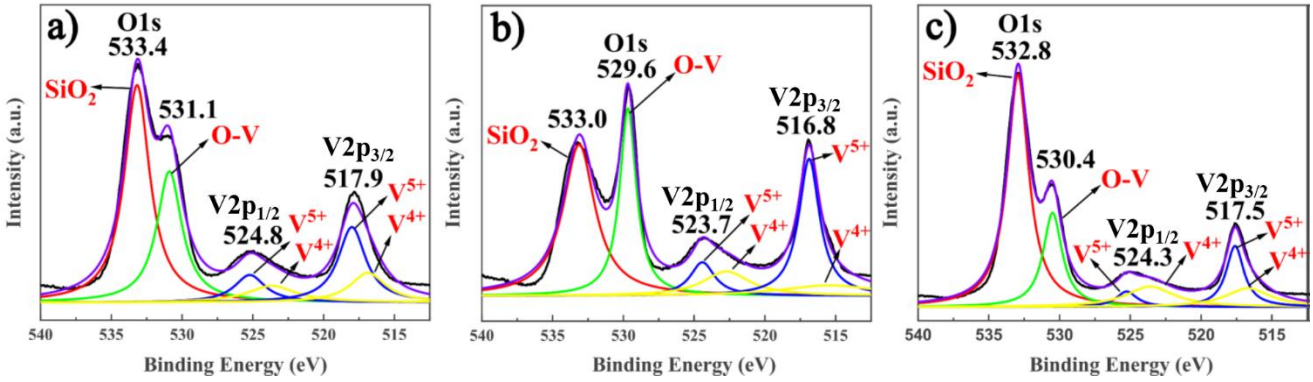

Figure 3. High resolution XPS spectra (O1s and V2p regions) for films deposited at laser fluences of: a) 7.3 J/cm^2, b)13.3 J/cm^2 and c)30.6 J/cm^2.

For the 30.6 J/cm² film (Figure 3c), the substrate (Si–O) signal is the most intense among the three samples, while the vanadium signals behave similarly to the other spectra. The Si signal likely arises from film discontinuities that expose the glass substrate, consistent with SEM and Raman observations.

3.4. Optical properties

Diffuse reflectance UV-Vis spectroscopy was selected because needle-, bar-, and droplet-like morphologies act as scattering centers for incident light (Murphy, 2007). The spectra shown in Figure 4 reveals an absorption edge beginning at approximately 340 nm and a broad band from ~500 to 700 nm consistent with previous reports (Abdullahi et al., 2016). Optical band gaps were estimated using the Kubelka-Munk (K-M) function and Tauc plots (Tauc *et al.*, 1966; Abdullahi *et al.*, 2016). Figure 5 shows Tauc plots for the film deposited at 30.6 J/cm² considering both indirect and direct band transitions. For an indirect transition, two linear regions yield two bandgap values; for a direct transition, only one value is obtained.

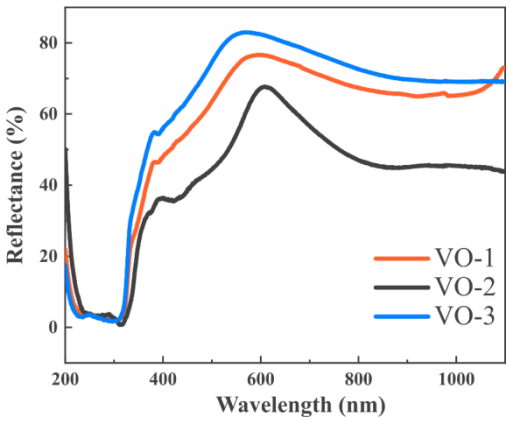

Figure 4. UV-Vis diffuse reflectance spectra for samples deposited at 7.3 J/cm^2 (VO-1), 13.3 J/cm^2 (VO-2), and 30.6 J/cm^2 (VO-3).

The calculated band gap values are shown in Table 1. Direct transitions values (~ 3.2 eV) do not match reported values for the phases present in the films. Reported band gaps for V_2O_5 are ~ 2.4 (direct) and ~2.0 eV (indirect); for single-walled V_2O_5 nanotubes, the band gap decreases as tube diameter decreases. For semiconducting VO_2 values of 0.6-0.7 eV have been reported (Parker *et al.*, 1990; Chain, 1991; Ivanovskaya *et al.*, 2003; Murphy, 2007). When indirect transitions are considered, the obtained values are closer to literature.

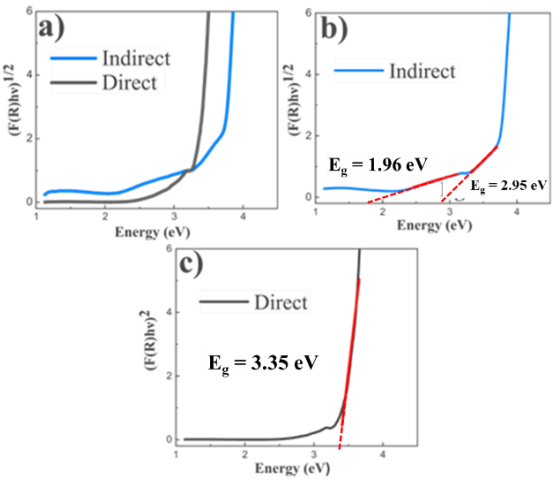

Figure 5. Tauc plots (Kubelka–Munk) for the 30.6 J/cm² film: (a) indirect vs direct comparison; (b) indirect extrapolation; (c) direct extrapolation.

Table 1. Band gap values from diffuse reflectance UV-Vis spectra.

Laser fluence (J/cm^2)	Band gap (eV)		
	Direct	Indirect	
7.3	3.25	2.91	1.74
13.3	3.20	2.19	1.64
30.6	3.35	2.95	1.96

Figure 6 shows the photoluminescence emission spectra of the deposited films excited with a wavelength of 500 nm. Three emission lines at 544 nm (2.28 eV), 655 nm (1.89 eV) and 730 nm (1.70 eV) for the three films are observed. The 655, and 730 nm emissions can be attributed to split off conduction bands of V_2O_5 due to its layered structure (Wang *et al*., 2021).

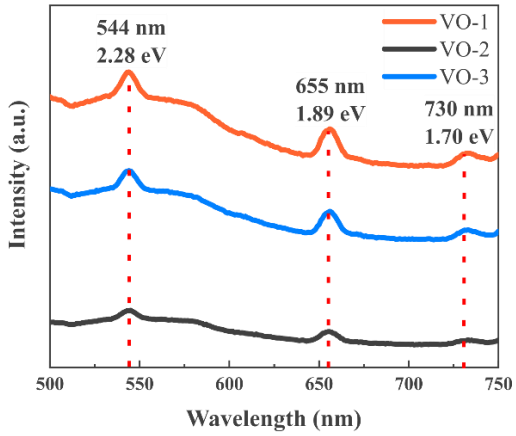

Figure 6. Photoluminescence spectra of the films deposited at 7.3 J/cm^2 (VO-1), 13.3 J/cm^2 (VO-2), and 30.6 J/cm^2 (VO-3).

4. Conclusions

Thin films composed of mixtures of vanadium oxides were obtained by PLD. The multiple oxidation states of vanadium favor the formation of different oxides, including nanotubular structures with mixed oxidation states. Raman and XPS reveal the presence of V_2O_5, VO_2 and possibly vanadium oxide nanotubes; $NaVO_3$) and SiO_2 were also detected. XPS shows V_2O_5 as the predominant phase, consistent of the higher stability of V^{5+} under these conditions. SEM reveals microneedles and microbars on the film surfaces. The employed approach enables obtaining V_2O_5 and VO_2 from metallic vanadium without hazardous chemical reagents. These thin film vanadium oxides have potential applications in catalysis, solar cells, smart windows, and optoelectronics.

References

Abdullahi, S. et al. (2016) 'Sımple Method For The Determınatıon of Band Gap of a Nanopowdered Sample Usıng Kubelka Munk Theory', Journal of the Nigerian Association of Mathematical Physics, 35, pp. 241–246.

Aburas, M. et al. (2019), Thermochromic smart window technologies for building application: A review. *Applied Energy*, 255, p. 113522. https://doi.org/https://doi.org/10.1016/j.apenergy.2019.113522.

Aita, C.R. et al. (1986), Optical behavior of sputter-deposited vanadium pentoxide. *Journal of Applied Physics*, 60(2), pp. 749–753. https://doi.org/10.1063/1.337425.

Bahlawane, N. and Lenoble, D. (2014), Vanadium Oxide Compounds: Structure, Properties, and Growth from the Gas Phase. *Chemical Vapor Deposition*, 20(7-8–9), pp. 299–311. https://doi.org/https://doi.org/10.1002/cvde.201400057.

Bannuru, T. et al. (2008), The electrical and mechanical properties of Au–V and Au–V2O5 thin films for wear-resistant RF MEMS switches. *Journal of Applied Physics*, 103(8), p. 83522. https://doi.org/10.1063/1.2902954.

Barceloux, D.G. and Barceloux, D. (1999), Vanadium. *Journal of Toxicology: Clinical Toxicology*, 37(2), pp. 265–278. https://doi.org/10.1081/CLT-100102425.

Blum, R.-P. et al. (2007), Surface Metal-Insulator Transition on a Vanadium Pentoxide (001) Single Crystal. *Physical Review Letters*, 99(22), p. 226103. https://doi.org/10.1103/PhysRevLett.99.226103.

Chain, E.E. (1991), Optical properties of vanadium dioxide and vanadium pentoxide thin films. *Applied Optics*, 30(19), pp. 2782–2787. https://doi.org/10.1364/AO.30.002782.

Chen, C.Y. et al. (2019), Vanadium Oxide as Transparent Carrier-Selective Layer in Silicon Hybrid Solar Cells Promoting Photovoltaic Performances. *ACS Applied Energy Materials*, 2(7), pp. 4873–4881. https://doi.org/10.1021/acsaem.9b00565.

Escobar-Alarcón, L., D.A. Solis-Casados, S. Romero, E. Haro-Poniatowski (2024), TiO_2-Fe_2O_3 binary thin films prepared by magnetron sputtering for photocatalytic applications. *Materials Science and Engineering B*, 302, 117261.

Escobar-Alarcón, L., E. Camps, M.A. Castro, S. Muhl, J. A. Mejia-Hernandez (2005), Effect of the plasma parameters on the properties of titanium nitride thin films grown by laser ablation. *Applied Physics A*, 81 (6), pp 1221-1226.

Gonzalez-Zavala, F. et al. (2016), Preparation of vanadium oxide thin films modified with Ag using a hybrid deposition configuration. *Applied Physics A: Materials Science and Processing*, 122(4), pp. 1–6. https://doi.org/10.1007/s00339-016-9991-0.

Hu, Peng et al. (2023), Vanadium Oxide: Phase Diagrams, Structures, Synthesis, and Applications. *Chemical Reviews*, 123(8), pp. 4353–4415. https://doi.org/10.1021/acs.chemrev.2c00546.

Ivanovskaya, V. V et al. (2003), Electronic properties of single-walled V_2O_5 nanotubes. *Solid State Communications*, 126(9), pp. 489–493. https://doi.org/https://doi.org/10.1016/S0038-1098(03)00254-0.

Julien, C., E. Haro-Poniatowski, L. Escobar-Alarcón, M.A. Camacho-López, J. Jimenez-Jarquin (1999), Growth of V_2O_5 thin films by pulsed laser deposition and their applications in lithium microbatteries. *Materials Science and Engineering B*, 63, 170-176.

Julien, C., Nazri, G.A. and Bergström, O. (1997), Raman Scattering Studies of Microcrystalline V_6O_{13}, *Physica status solidi (b)*, 201(1), pp. 319–326. https://doi.org/https://doi.org/10.1002/1521-3951(199705)201:1<319::AID-PSSB319>3.0.CO;2-T.

Liu, A. et al. (2007), Vanadium-oxide nanotubes: Synthesis and template-related electrochemical properties. *Electrochemistry Communications*, 9(7), pp. 1766–1771. https://doi.org/https://doi.org/10.1016/j.elecom.2007.03.027.

Liu, X. et al. (2006), The effect of thermal annealing and laser irradiation on the microstructure of vanadium oxide nanotubes. *Applied Surface Science*, 253(5), pp. 2747–2751. https://doi.org/https://doi.org/10.1016/j.apsusc.2006.05.041.

Mai, L. et al. (2011), Vanadium oxide nanowires for Li-ion batteries. *Journal of Materials Research*. 2011/07/13, 26(17), pp. 2175–2185. https://doi.org/DOI: 10.1557/jmr.2011.171.

Mendialdua, J., Casanova, R. and Barbaux, Y. (1995), XPS studies of V_2O_5, V_6O_{13}, VO_2 and V_2O_3. *Journal of Electron Spectroscopy and Related Phenomena*, 71(3), pp. 249–261. https://doi.org/https://doi.org/10.1016/0368-2048(94)02291-7.

Morales Méndez, J. G, B. A. Macías Ayala, A. A. Aguilar Cardoso, J. G. Limas González, L. Escobar Alarcón, M. Picquart, E. Haro Poniatowski (2023), Surface Enhanced Raman Spectroscopy of Methylene Blue Deposited on Ag Nanostructured Substrates prepared by PLD. *Vacuum*, 207: 111580.

Moulder, J.F. et al. (1992), Handbook of X-ray Photoelectron Spectroscopy: A reference book of standard spectra for identification and interpretation of XPS data. Eden Prairie, Minnesota: Physical Electronics Division, Perkin-Elmer Corporation, p. 261.

Muhr, H.-J. et al. (2000), Vanadium Oxide Nanotubes—A New Flexible Vanadate Nanophase. *Advanced Materials*, 12(3), pp. 231–234. https://doi.org/https://doi.org/10.1002/(SICI)1521-4095(200002)12:3<231::AID-ADMA231>3.0.CO;2-D.

Murphy, A.B. (2007), Band-gap determination from diffuse reflectance measurements of semiconductor films, and application to photoelectrochemical water-splitting. *Solar Energy Materials and Solar*

Cells, 91(14), pp. 1326–1337. https://doi.org/10.1016/j.solmat.2007.05.005.

Neuville, D.R. (2006), Viscosity, structure and mixing in (Ca, Na) silicate melts. *Chemical Geology*, 229(1), pp. 28–41. https://doi.org/https://doi.org/10.1016/j.chemgeo.2006.01.008.

Pan, M. et al. (2004), Raman study of the phase transition in VO_2 thin films. *Journal of Crystal Growth*, 268(1), pp. 178–183. https://doi.org/https://doi.org/10.1016/j.jcrysgro.2004.05.005.

Parker, J.C. et al. (1990), Optical properties of vanadium pentoxide determined from ellipsometry and band-structure calculations. *Physical Review B*, 42(8), pp. 5289–5293. https://doi.org/10.1103/PhysRevB.42.5289.

Pooseekheaw, P. et al. (2022), Effect of magnetic field on improvement of photocatalytic performance of V_2O_5/TiO_2 nanoheterostructure films prepared by sparking method. *Scientific Reports*, 12(1), p. 2298. https://doi.org/10.1038/s41598-022-05015-2.

Salamati, M. et al. (2019), Preparation of TiO_2@W-VO_2 thermochromic thin film for the application of energy efficient smart windows and energy modeling studies of the produced glass. *Construction and Building Materials*, 218, pp. 477–482. https://doi.org/10.1016/j.conbuildmat.2019.05.046.

Schilbe, P. (2002), Raman scattering in VO_2. *Physica B: Condensed Matter*, 316–317, pp. 600–602. https://doi.org/https://doi.org/10.1016/S0921-4526(02)00584-7.

Selvakumar, N. and Barshilia, H.C. (2012), Review of physical vapor deposited (PVD) spectrally selective coatings for mid- and high-temperature solar thermal applications. *Solar Energy Materials and Solar Cells*, 98, pp. 1–23. https://doi.org/https://doi.org/10.1016/j.solmat.2011.10.028.

Souza Filho, A.G. et al. (2004), Raman Spectra in Vanadate Nanotubes Revisited. *Nano Letters*, 4(11), pp. 2099–2104. https://doi.org/10.1021/nl0488477.

Tauc, J., Grigorovici, R. and Vancu, A. (1966), Optical Properties and Electronic Structure of Amorphous Germanium. *Physica statu solidi (b)*, 15(2), pp. 627–637. https://doi.org/10.1002/pssb.19660150224.

Théry, V. et al. (2016), Role of thermal strain in the metal-insulator and structural phase transition of epitaxial VO_2 films. *Physical Review B*, 93(18), p. 184106. https://doi.org/10.1103/PhysRevB.93.184106.

Ureña-Begara, F., Crunteanu, A. and Raskin, J.-P. (2017), Raman and XPS characterization of vanadium oxide thin films with temperature. *Applied Surface Science*, 403, pp. 717–727. https://doi.org/https://doi.org/10.1016/j.apsusc.2017.01.160.

Utegulov, Z.N. et al. (2003), Structural characterization of Eu_2O_3–MgO–Na_2O–Al_2O_3–SiO_2 glasses with varying Eu_2O_3 content: Raman and NMR studies. *Journal of Non-Crystalline Solids*, 315(1), pp. 43–53. https://doi.org/https://doi.org/10.1016/S0022-3093(02)01594-6.

Wang, C. C. et al. (2021), Structure and Photoluminescence Properties of Thermally Synthesized V_2O_5 and Al-Doped V_2O_5 Nanostructures. *Materials 14(2), 359*. https://doi.org/10.3390/ma14020359.

Wang, N. et al. (2016)y, Terbium-Doped VO_2 Thin Films: Reduced Phase Transition Temperature and Largely Enhanced Luminous Transmittancey. *Langmuir*, 32(3), pp. 759–764. https://doi.org/10.1021/acs.langmuir.5b04212.

Zhang, Y. et al. (2012), Preparation of W- and Mo-doped VO_2(M) by ethanol reduction of peroxovanadium complexes and their phase transition and optical switching properties. *Journal of Alloys and Compounds*, 544, pp. 30–36. https://doi.org/https://doi.org/10.1016/j.jallcom.2012.07.093.

Zhou, Q. et al. (2020), Boron doped M-phase VO_2 nanoparticles with low metal-insulator phase transition temperature for smart windows. *Ceramics International*, 46(4), pp. 4786–4794. https://doi.org/https://doi.org/10.1016/j.ceramint.2019.10.211.